Giner-Sanz, JJ.; Ortega Navarro, EM.; García-Gabaldón, M.; Pérez-Herranz, V. (2018). Theoretical Determination of the Stabilization Time in Galvanostatic EIS Measurements: The Simplified Randles Cell. Journal of The Electrochemical Society. 165(13):E628-E636. https://doi.org/10.1149/2.0271813jes

Theoretical determination of the stabilization time in galvanostatic EIS measurements. The simplest case: the simplified Randles cell

J. J. Giner-Sanz, E. M. Ortega, M. García-Gabaldón, V. Pérez-Herranz*
IEC group, Depto. Ingeniería Química y Nuclear, Universitat Politècnica de València
Camino de Vera S/N, 46022 Valencia, Spain
*Corresponding author. Tel.: +34-96-3877632; fax: +34-96-3877639;
E-mail address: vperez@iqn.upv.es (V. Pérez-Herranz)

Abstract:

Usually, EIS measurements are performed in 2 steps: a stabilization step followed by an acquisition step. The first is necessary in order to ensure that the impedance is determined when the system has reached its stationary state. In this work, a theoretical framework is proposed for estimating the required stabilization time for EIS measurements. Here, it was applied to the simplest case: the simplified Randles cell. In order to calculate the required stabilization time for performing EIS measurements, a theoretical dynamic model of a Randles cell under galvanostatic sinusoidal perturbation was developed. The proposed model can be used to estimate, from a theoretical point of view, the required stabilization time for performing EIS measurements in a Randles-like system. Even though, this work focuses on the simplest case, the developed theoretical framework can be applied to any system, however complex it may be.

Keywords: Electrochemical impedance spectroscopy (EIS), Stabilization time, Electrochemical system dynamics, Theoretical modelling, Simplified Randles circuit.

1. Introduction

Electrochemical impedance spectroscopy (EIS) is a non-destructive electrochemical method, with a broad range of applications in different fields of electrochemical science and engineering, among which are, for example, energy storage [1-2], batteries [3-8], electrochemical sensors [9-12], fuel cells [13-18], electrolysers [19-21], corrosion and coatings [22-25], and bioelectrochemistry [26, 27]. The power of this electrochemical technique arises from its ability to distinguish the different physic-chemical processes undergoing at different timescales in the system [28]. This ability makes EIS a perfect tool for studying the mechanisms of electrochemical reactions, the electric and transport properties of materials, and complex interfaces [29].

The EIS technique consists in applying an electrical sinusoidal signal (current or potential) of known frequency and amplitude to an electrochemical system, while the amplitude and the phase of the output signal (potential or current) are monitored [30]. From these 2 parameters, the impedance of the system at the applied frequency is calculated using generalized Ohm's law. The impedance concept is a generalization of the DC electric resistance concept: it encapsulates information on both, the electric resistance of the system (i.e. amplitude relation between the current and the voltage signals) and the time offset between the signals [31]. In general, the impedance is not measured at only one frequency. Instead, a frequency sweep is usually performed: the impedance measurement is done sequentially for different perturbation frequencies [32]; hence the name “spectroscopy” [33].

The common practice is to perform the EIS measurement for each excited frequency in 2 steps: a stabilization step followed by an acquisition step [34]. During the stabilization step, the perturbation is applied but the signals are not acquired; whereas during the acquisition step, the signals are acquired and the impedance is determined. The stabilization step is necessary in order to ensure that when the signals are acquired (and the impedance is calculated), the system is in its stationary state. It should be noted that, from a mathematical point of view, the stationary state concept is slightly different from the steady state one. On the one hand, in a steady state, the system variables are constant with time (i.e. $\neq f(t)$). On the other hand, in a stationary state, the system variables may present temporal variations (i.e. $= f(t)$), but their variation patterns repeat themselves in time. According to these definitions, a steady state is a particular case of stationary state, but not all stationary states are steady states. Since in EIS context both signals (perturbation and output signals) are sinusoidal signals, the system variables change in time, and therefore, no proper steady state is reached during an EIS measurement. Conversely, in an EIS measurement the system reaches a stationary state: after a certain time, the signals display a cycle that repeats itself cyclically over time. The system is considered to be in

a stationary state, when one cycle overlaps with the previous one. The stabilization step has to be long enough in order to ensure that the system reaches its stationary state before the acquisition starts.

In general, when a new system is going to be analysed using EIS, no preliminary study is done in order to determine the required duration of the stabilization step for guaranteeing that the system has reached the stationary state before starting the acquisition step [35]. Some of the common practices for the selection of the stabilization time are using the default settings provided by the software used to perform the EIS measurement, or using the parameters available in literature for similar systems [36]. However, these practices may lead to an inadequately short stabilization step. In this case, the acquisition starts before the stationary state is reached, which results in an erroneous determination of the impedance.

In literature, some works [36, 37] deal with the selection of the measurement parameters, that include the parameters that define the stabilization step duration, for EIS measurements. These works use an experimental approach. To the best of the authors' knowledge, there are no previous works in literature that study the stabilization time in EIS measurements from a theoretical point of view. The present work intends to partially fill this gap in the literature: A theoretical framework is proposed for estimating the required stabilization time for EIS measurements of a particular electrochemical system. Since this work is a first approach to the problem, the simplest system was considered: the simplified Randles cell (i.e. Randles circuit with no mass transport limitation). The simplified Randles cell is a particular case of the Randles cell, which is a well-known equivalent electric circuit (EEC) that models a semi-infinite diffusion-controlled faradaic reaction to a planar electrode [35]. The Randles cell consists of an electrolyte resistance, R_0, in series with the parallel combination of the double-layer capacitance, C_{dl}, and the impedance of a faradaic reaction. J.E.B. Randles proposed to model the faradic impedance as an active charge transfer resistance in series with a Warburg element, related to mass transport [38]. Conversely, in the simplified Randles cell, the faradic impedance is modelled only by a charge transfer resistance.

In spite of its simplicity, the Simplified Randles cell is one of most common electrochemical cell models: it has been used to model a vast range of electrochemical systems [39]. For example, Ribeiro and co-workers proposed a Randles CCE to model concrete corrosion [40]; while Liu's group [41] and Li's group [42] used it for modelling respectively, carbon steel and aluminium alloy corrosion. Randles cell has also been used for modelling electrochemical electrodes, such as nickel oxide nanoparticles modified glassy carbon electrode [43], polycrystalline rhenium electrodes [44], and IB/VIB family electrodes [45]. It has been used to model fuel cells: Pérez-Page and

Pérez-Herranz used it to model a PEM fuel cell stack [46], Sindhuja and co-workers modelled a microbial fuel cell with a Randles EEC [47], and Cruz-Manzo's group used it to build a fuel cell cathodic catalyst layer model [48]. Furthermore, Randles cell has been used for modelling ionic liquid systems, such as a surfactant/salt/water ternary system [49], and an ionic liquid/oil interface [50]. Finally, some examples of exotic systems that have been modelled using the Randles EEC can be found in literature: carbon nanotube cement-based composites [51], a viologen-based electrochromic device [52], SiO_2 layers [53], and the gum Arabic-Chitosan complexation process in bulk solution [54]. These are just some of the countless examples of the application of the Randles cell, available in literature. In addition to being a useful model in its own right, the simplified Randles cell is the starting point for other more complex models [55]. The combination of its simplicity and its usefulness, make the simplified Randles cell the perfect candidate for this work.

This work's goal is to build a theoretical dynamic model of a Randles cell under galvanostatic sinusoidal perturbation, in order to derive from it the required stabilization time for performing EIS measurements. After developing the model, a sensitivity analysis will be performed in order to study the effect of the different parameters of the Randles cell on the required stabilization time. Finally, the obtained results will be transposed to examples of real experimental systems extracted from literature, in order to obtain an estimation of the order of magnitude of the required stabilization time for performing EIS measurements in these example systems.

2. Dynamic model and stabilization time

2.1. Characteristic ODE of the simplified Randles cell

The simplified Randles cell is formed by 3 circuit elements: an electrolyte resistance, R_0, in series with the parallel combination of the double-layer capacitance, C_{dl}, and the charge transfer resistance, R_{ct}. Figure 1 defines the parameters and the variables of the simplified Randles cell. On the one hand, this system has 3 parameters: R_0, R_{ct} and C_{dl}. By the nature of these parameters, it can be assumed without loss of generality that they are all three, non-zero positive numbers ($R_0 > 0$, $R_{ct} > 0$ and $C_{dl} > 0$). Furthermore, assuming that the system is temporarily stable, the 3 parameters can be considered constant with time. Thus, in the context of this work, R_0, R_{ct} and C_{dl} are non-zero positive constants. On the other hand, 2 variables are associated to each circuit element: the current that crosses the element, and the potential difference (i.e. voltage) between its terminals. Additionally, 2 more variables are required for defining the whole cell: the total current and the total voltage. All these variables are defined according to the conventions shown in figure 1.

First, according to Kirchhoff's voltage law (KVL):

$$U_{Rct} = U_C \equiv U_{RC} \tag{1}$$

$$U_{tot} = U_{R0} + U_{RC} \tag{2}$$

Second, according to Kirchhoff's current law (KCL):

$$I_{tot} = I_{R0} = I_{Rct} + I_C \tag{3}$$

Third, applying Ohm’s law to both resistances:

$$U_{R0} = I_{R0} \cdot R_0 \tag{4}$$

$$U_{Rct} = I_{Rct} \cdot R_{ct} \tag{5}$$

Finally, since C_{dl} is constant with time, according to the derivative form of the current–voltage relation of a capacitor:

$$I_C = C_{dl} \cdot \frac{dU_C}{dt} \tag{6}$$

Where $\frac{d\therefore}{dt}$ denotes the time derivative operator. Combining equations (1), (3), (5) and (6), the following expression is obtained:

$$I_{tot} = \frac{U_{RC}}{R_{ct}} + C_{dl} \cdot \frac{dU_{RC}}{dt} \tag{7}$$

Combining equations (2) and (4):

$$U_{RC} = U_{tot} - I_{tot} \cdot R_0 \tag{8}$$

Introducing equation (8) in equation (7), and using the fact that the derivative operator is a linear operator (and R_0 is a constant):

$$I_{tot} = \frac{U_{tot}}{R_{ct}} - \frac{R_0}{R_{ct}} \cdot I_{tot} + C_{dl} \cdot \frac{dU_{tot}}{dt} - C_{dl} \cdot R_0 \cdot \frac{dI_{tot}}{dt} \tag{9}$$

The characteristic ordinary differential equation (ODE) of the simplified Randles cell was obtained by rearranging expression (9):

$$C_{dl} \cdot \frac{dU_{tot}}{dt} + \frac{1}{R_{ct}} \cdot U_{tot} = \left(1 + \frac{R_0}{R_{ct}}\right) \cdot I_{tot} + C_{dl} \cdot R_0 \cdot \frac{dI_{tot}}{dt} \tag{10}$$

2.2. The Cauchy problem associated to the simplified Randles cell under galvanostatic sinusoidal perturbation

In galvanostatic EIS measurements, the perturbation signal is a mono-frequency sinusoidal current signal. In addition, generally, a polarization current (i.e. DC component) is applied as well. Therefore, the most general galvanostatic sinusoidal perturbation can be defined as a superposition of a DC component and a sinusoidal signal:

$$I_{tot}(t) = I_{DC} + \Delta I \cdot \sin(\omega \cdot t) \tag{11}$$

Where I_{DC} denotes the polarization current, ΔI is the perturbation amplitude, $\omega = 2\pi \cdot f$ represents the angular frequency of the perturbation, and f is the frequency of the perturbation. ΔI can be considered as a nonzero positive constant, with no loss of generality. Applying the differentiation rules to the last expression:

$$\frac{dI_{tot}}{dt}(t) = \Delta I \cdot \omega \cdot \cos(\omega \cdot t) \tag{12}$$

The general convention in RC circuits is to define the following time constant: $\tau_{RC} = C_{dl} \cdot R_{ct}$. Multiplying both members of the characteristic ODE of the simplified Randles cell (equation (10)) by R_{ct}, introducing expressions (11) and (12), and replacing the previously defined time constant, the following expression was obtained:

$$\begin{aligned}\tau_{RC} \cdot \frac{dU_{tot}}{dt} + U_{tot} \\ = (R_{ct} + R_0) \cdot I_{DC} + (R_{ct} + R_0) \cdot \Delta I \cdot \sin(\omega \cdot t) + \tau_{RC} \cdot R_0 \\ \cdot \Delta I \cdot \omega \cdot \cos(\omega \cdot t)\end{aligned} \tag{13}$$

The right hand term is a linear combination of a sine and a cosine of same frequency. It is well-known that any linear combination of cosines and sines of equal period is equal to a single sine with the same period but with different amplitude and with a phase shift [56]:

$$c_1 \cdot \cos(\omega \cdot t) + c_2 \cdot \sin(\omega \cdot t) = A \cdot \sin(\omega \cdot t + \phi) \tag{14}$$

Where, for $c_2 \neq 0$:

$$A = \sqrt{c_1^2 + c_2^2} \tag{15}$$

$$\phi = arctan2(c_1; c_2) \tag{16}$$

$arctan2$ denotes the arctan function generalized on the 4 quadrants. For eliminating any ambiguity, this function uses the principal value of the returned angles: $-\pi < arctan2(c_1; c_2) \leq \pi$. The $arctan2$ can be defined in terms of the standard $arctan$ function as follows:

$$arctan2(c_1; c_2) = \begin{cases} arctan\left(\frac{c_1}{c_2}\right) & if\ c_2 > 0 \\ arctan\left(\frac{c_1}{c_2}\right) + \pi & if\ c_2 < 0\ and\ c_1 \geq 0 \\ arctan\left(\frac{c_1}{c_2}\right) - \pi & if\ c_2 < 0\ and\ c_1 < 0 \\ +\frac{\pi}{2} & if\ c_2 = 0\ and\ c_1 > 0 \\ -\frac{\pi}{2} & if\ c_2 = 0\ and\ c_1 < 0 \end{cases} \tag{17}$$

Using the above result, the right member of equation (13) can be expressed in its amplitude-phase form:

$$\tau_{RC} \cdot \frac{dU_{tot}}{dt} + U_{tot} = (R_{ct} + R_0) \cdot I_{DC} + A_{RRC} \cdot \sin(\omega \cdot t + \phi_{RRC}) \quad (18)$$

With:

$$A_{RRC} = \Delta I \cdot \sqrt{(R_{ct} + R_0)^2 + \tau_{RC}^2 \cdot R_0^2 \cdot \omega^2} \quad (19)$$

$$\phi_{RRC} = arctan\left(\frac{\tau_{RC} \cdot R_0 \cdot \omega}{R_{ct} + R_0}\right) \quad (20)$$

Once the ODE of the system has been fully defined, the next step is to define the initial conditions. Since ODE (18) is a first order ODE, only one initial condition is required. At this point, two cases must be distinguished: the first applied perturbation (i.e. the first frequency) and the rest of the applied perturbations. The common practice for performing EIS measurements is to polarize the system before starting to apply the different perturbations [35]. This means that initially only I_{DC} is applied to the system. After a certain time, the system's voltage will reach its DC level, U_{DC}. Once the system is polarized ($I = I_{DC}$ and $U = U_{DC}$), the first perturbation (i.e. first frequency) is applied. Therefore, considering $t = 0$ as the time when the perturbation is applied, for the first perturbation: $U_{tot}(0) = U_{DC}$. On the contrary, for the following perturbations, the perturbation is applied directly after the end of the acquisition stage of the previous frequency (i.e. abrupt change in the frequency). In general, an integer number of cycles is acquired during the acquisition stage [36]. Therefore, if the system is stable (i.e. no time drift), the end point of the acquisition stage is the same point as the initial point of the stabilization stage ($U = U_{DC}$). So, considering $t = 0$ as the time when the new perturbation is applied, for the all the perturbations applied after the first one: $U_{tot}(0) = U_{DC}$. Since the initial conditions associated to both cases (first perturbation and non-first perturbations) are the same, a unique initial condition can be considered:

$$U_{tot}(0) = U_{DC} \quad (21)$$

This initial condition defines completely the initial value problem. The Cauchy problem associated to the simplified Randles cell under galvanostatic sinusoidal perturbation can be written as:

$$\begin{cases} \tau_{RC} \cdot \dfrac{dU_{tot}}{dt} + U_{tot} = (R_{ct} + R_0) \cdot I_{DC} + A_{RRC} \cdot \sin(\omega \cdot t + \phi_{RRC}) \\ U_{tot}(0) = U_{DC} \end{cases} \quad (22)$$

Where A_{RRC} and ϕ_{RRC} are defined by equations (19) and (20) respectively. These constants depend on the cell's parameters (R_0, R_{ct} and C_{dl}) and on the perturbation's parameters (ΔI and ω): A_{RRC} and ϕ_{RRC} are constant with respect to t and U_{tot}. Therefore, the ODE of the aforementioned Cauchy problem is a first order, linear, non-homogeneous, non-autonomous ODE with constant coefficients.

2.3. Solution of the Cauchy problem

The first order ODE of Cauchy problem (22) can be rewritten in the form:

$$\frac{dU_{tot}}{dt} = f(t, U_{tot}(t)) \quad (23)$$

Where $f(t, U) = -\frac{1}{\tau_{RC}} \cdot U + \frac{A_{RRC}}{\tau_{RC}} \cdot \sin(\omega \cdot t + \phi_{RRC}) + \frac{R_{ct}+R_0}{\tau_{RC}} \cdot I_{DC}$. This function is uniformly Lipschitz continuous in U, and continuous in t. Applying Picard-Lindelöf theorem [57] (also known as Cauchy-Lipschitz theorem) of the existence and uniqueness of solutions to initial value problems with first-order differential equations, it can be concluded that the solution $U_{tot}(t)$ to (22) exists and is unique on an open interval centered at t_0 (0 in this case).

Since the ODE is a linear non-homogeneous ODE, its general solution can be written as the superposition of the general solution of the associated homogeneous ODE, U_h, and a particular solution of the non-homogeneous ODE, U_p [58]:

$$U_{tot}(t) = U_h(t) + U_p(t) \quad (24)$$

On the one hand, the associated homogeneous ODE is a simple first order ODE with constant coefficients. Its characteristic polynomial, $p(\lambda) = \tau_{RC} \cdot \lambda + 1$, has a single root: $-1/\tau_{RC}$. Since by assumption, $\tau_{RC} > 0$, the root of the characteristic polynomial is a real negative root. Therefore, the system is dynamically stable, and the general solution of the homogeneous ODE is:

$$U_h(t) = \beta \cdot e^{-\frac{t}{\tau_{RC}}} \quad (25)$$

With $\beta \in \mathbb{R}$.

On the other hand, since the non-homogeneous term is a superposition of a sinusoidal function and a constant term, the ODE is sinusoidally forced. ODEs with sinusoidal forcing can be solved by complexification (i.e. complex replacement technique). In this case, using the aforementioned technique, the following particular solution was obtained:

$$U_p(t) = (R_0 + R_{ct}) \cdot I_{DC} + \frac{\Delta I}{\omega^2 \cdot \tau_{RC}^2 + 1} \cdot [(R_0 + R_{ct} + \tau_{RC}^2 \cdot R_0 \cdot \omega^2) \cdot sin(\omega \cdot t) - \tau_{RC} \cdot \omega \cdot R_{ct} \cdot \cos(\omega \cdot t)] \quad (26)$$

The general solution of the ODE was obtained by introducing expressions (25) and (26) in (24). Then, using the initial condition, the value of β was determined; obtaining in this way the unique solution of the Cauchy problem. The obtained solution can be grouped into 3 terms:

$$U_{tot}(t) = U_{DC} + U_{SS}(t) + U_{trans}(t) \quad (27)$$

Where:

$$U_{DC} = (R_0 + R_{ct}) \cdot I_{DC} \quad (28)$$

$$U_{SS}(t) = \frac{\Delta I}{\omega^2 \cdot \tau_{RC}^2 + 1} \cdot [(R_0 + R_{ct} + \tau_{RC}^2 \cdot R_0 \cdot \omega^2) \cdot sin(\omega \cdot t) - \tau_{RC} \cdot \omega \cdot R_{ct} \cdot \cos(\omega \cdot t)] \quad (29)$$

$$U_{trans}(t) = \frac{\Delta I \cdot \tau_{RC} \cdot R_{ct} \cdot \omega}{\omega^2 \cdot \tau_{RC}^2 + 1} \cdot e^{-\frac{t}{\tau_{RC}}} \quad (30)$$

For physical reasons, the above expressions are only valid for $t \geq 0$ (i.e. time forward hypothesis).

On the one hand, U_{DC} is the DC component of the output signal. It corresponds with the response of the system to the DC component of the perturbation signal. From a DC point of view, C_{dl} behaves as an open circuit, and the Randles circuit reduces to the series combination of two resistors, R_0 and R_{ct}. This is consistent with the obtained expression for U_{DC} (expression 28). On the other hand, taking limits in equation (27):

$$\lim_{t \to +\infty} U_{tot}(t) - \big(U_{DC} + U_{SS}(t)\big) = 0 \quad (31)$$

The immediate interpretation of the above result is that, in the "long term", $U_{tot}(t)$ tends to $U_{DC} + U_{SS}(t)$. Therefore, a stationary state is reached, and the system's output in this stationary state is $U_{DC} + U_{SS}(t)$. Since U_{DC} is the DC component, $U_{SS}(t)$ is the stationary AC component of the output signal. The obtained expression for $U_{SS}(t)$ (equation (29)) is consistent with the well-known expression of the complex impedance, Z, of a simplified Randles circuit [59]:

$$Z(\omega) = \left(R_0 + \frac{R_{ct}}{\omega^2 \cdot \tau_{RC}^2 + 1}\right) + j \cdot \left(-\frac{\tau_{RC} \cdot \omega \cdot R_{ct}}{\omega^2 \cdot \tau_{RC}^2 + 1}\right) \quad (32)$$

Where $j = \sqrt{-1}$ denotes the imaginary unit.

Finally, $U_{trans}(t)$ is the transient component of the output signal. As it can be seen in expression (30), this term vanishes with time, causing the convergence of $U_{tot}(t)$ to its corresponding stationary state. Therefore, $U_{trans}(t)$ is responsible for the transition of the system from its initial state to its stationary state.

Figure 2 shows the simulated results for an example Randles cell ($R_0 = 10\ m\Omega$, $R_{ct} = 40\ m\Omega$ and $C_{dl} = 450\ m\mathrm{F}$), and a perturbation of $1\ mA$ amplitude and $20\ Hz$ frequency. In the aforementioned figure, the results are displayed in 3 different spaces: in subfigure a, they are represented in the time space; in subfigure b, they are represented in the phase space; and finally, in subfigure c, they are represented in the Lissajous space. In the phase space and in the Lissajous space, the initial state of the system is marked with a black dot. On the one hand, in the time space, it can be observed that both signals, $I_{tot}(t)$ and $U_{tot}(t)$, are initially ($t = 0$) in their DC value: I_{DC} and U_{DC}, respectively. At $t = 0$, the sinusoidal perturbation is applied, causing the output voltage to start changing. After a certain amount of time, the $U_{tot}(t)$ signal converges completely to the stationary output. The AC component of this stationary output signal is a sinusoidal signal of the same frequency as the AC component of the perturbation signal. These AC components present an offset between them, and have different amplitudes. The amplitude ratio and the offset between the AC components in the stationary state define the impedance of the system at the excited frequency. Therefore, for a correct impedance measurement, the acquisition should start after the transient: once $U_{tot}(t)$ has converged to its stationary state. On the other hand, in the phase space and in the Lissajous space, the trajectory of the system starts in the initial state point and converges to the stationary ovoid, associated to the stationary state. In the Lissajous space, the stationary ovoid corresponds to the well-known, in the EIS context, clockwise-rotation ellipse.

2.4. Stabilization time

As stated in the introduction section, in the context of this work, the stabilization time is defined as the time required for the system to reach its stationary state. As given by expression (30), the transient component has a vanishing exponential relation with time. Figure 3 shows the simulated transient component for the example Randles cell and the perturbation considered in the previous section. In it, the vanishing exponential behaviour can be clearly observed. From a mathematical point of view, $U_{trans}(t)$ tends to 0 but it is never equal to 0. So, strictly speaking, the stabilization time is $+\infty$. However, from a practical point of view, convergence can be understood as been close enough, rather than been exactly equal. According to this idea, convergence can be defined using the threshold concept: the system will be said to have converged once the transient component falls below a certain threshold. In this system, a logical choice for the threshold is a certain percentage of the amplitude of the stationary AC component of the output signal, ΔU_{SS}. Obviously, using this definition does not lead to a unique stabilization time; instead, the stabilization time will be linked to the selected percentage, δ. Therefore, the stabilization time associated to threshold δ, τ_δ^S, is defined as the time for which the transient component is equal to corresponding percentage of ΔU_{SS}:

$$\frac{U_{trans}\left(\tau_\delta^S\right)}{\Delta U_{SS}} = \delta \qquad (33)$$

Where according to generalized Ohm's law:

$$\Delta U_{SS} = |Z(\omega)| \cdot \Delta I \qquad (34)$$

$|Z(\omega)|$ is the impedance modulus, that can be obtained by applying the complex modulus operator to equation (32).

In figure 3, the threshold associated to $\delta = 20\%$, and the one associated to $\delta = 5\%$, are superimposed to the transient component. The corresponding stabilization times are identified on the graphic. Evidently, a lower δ leads to a higher stabilization time: if the convergence criterion is more severe (i.e. the signal has to get closer to the stationary state), then more time is required for achieving convergence (i.e. larger τ_δ^S).

Introducing expressions (30) and (34) in (33), and algebraically operating with the resulting expression, the following equation was obtained for the stabilization time associated to δ threshold:

$$\tau_{\delta}^{S}(\omega) = -\tau_{RC} \cdot ln\left(\frac{\delta \cdot |Z(\omega)| \cdot (\omega^2 \cdot \tau_{RC}^2 + 1)}{\tau_{RC} \cdot R_{ct} \cdot \omega}\right) \quad (35)$$

The above expression is mathematically defined for all $\omega \epsilon \mathbb{R}^+$, since all the system parameters, δ and $|Z(\omega)|$ are real positive numbers. However, the above expression leads to physical inconsistencies for some ranges of ω: for these ω, the stabilization time calculated using equation (35) is negative, which obviously is not physically possible. These cases correspond to cases where the initial value of the transient, $U_{trans}(0)$, is already lower than the threshold. According to the convergence definition introduced in this work, $U_{trans}(0) \leq \delta \cdot \Delta U_{SS}$ implies that the system has already converged to its stationary state at $t = 0$. In this work, the following convention was adopted: if the system has already converged at $t = 0$, the stabilization time is considered to be 0. The $U_{trans}(0) = \delta \cdot \Delta U_{SS}$ condition (i.e. limit case) is equivalent to the following equation:

$$\delta \cdot |Z(\widetilde{\omega})| \cdot [(\widetilde{\omega})^2 \cdot \tau_{RC}^2 + 1] - \tau_{RC} \cdot R_{ct} \cdot \widetilde{\omega} = 0 \quad (36)$$

In this case, the above equation has 2 real positive solutions, which will be denoted as $\widetilde{\omega}_1$ and $\widetilde{\omega}_2$. Therefore, the stabilization time associated to the δ threshold for the simplified Randles cell is given by:

$$\tau_{\delta}^{S}(\omega) = \begin{cases} -\tau_{RC} \cdot ln\left(\dfrac{\delta \cdot |Z(\omega)| \cdot (\omega^2 \cdot \tau_{RC}^2 + 1)}{\tau_{RC} \cdot R_{ct} \cdot \omega}\right) & if\ \widetilde{\omega}_1 \leq \omega \leq \widetilde{\omega}_2 \\ 0 & otherwise \end{cases} \quad (37)$$

The stabilization time defined in this way is $\tau_{\delta}^{S}(\omega) \geq 0\ \forall \omega \in \mathbb{R}^+$, which is physically consistent with the definition of the stabilization time.

3. Analysis of the model

3.1. Effect of the perturbation frequency

Expression (37) can be used in order to calculate the δ-stabilization time as a function of the perturbation frequency $f = \omega \cdot (2\pi)^{-1}$. Figure 4 shows the obtained results for the 1% stabilization time, $\tau_{1\%}^{S}$, of the example Randles cell considered in the previous section ($\mathrm{R_0} = 10\ \mathrm{m\Omega}$, $\mathrm{R_{ct}} = 40\ \mathrm{m\Omega}$ and $\mathrm{C_{dl}} = 450\ \mathrm{mF}$). The curve presents a very characteristic shape. First, frequencies $\tilde{f}_1 = \tilde{\omega}_1 \cdot (2\pi)^{-1}$ and $\tilde{f}_2 = \tilde{\omega}_2 \cdot (2\pi)^{-1}$ delimit the frequency range for which the curve is non zero: as explained previously, for frequencies higher than $\tilde{f}_2$, or frequencies lower than $\tilde{f}_1$, the system has already converged (for a 1% threshold) to its stationary state at $t = 0$. Second, the curve presents a maximum: for some characteristic frequency, Λ, the δ-stabilization time is maximum. The maximum stabilization time for a δ threshold will be denoted as τ_{δ}^{max}. Λ and $\tau_{1\%}^{max}$ are identified on figure 4. Finally, the curve presents a nearly linear (in a semi-log plot) behaviour for frequencies far from the characteristic frequency. In the low frequency branch ($f_1 < f \ll \Lambda$), the curve presents a positive-slope linear behaviour; whereas, in the high frequency branch ($\Lambda \ll f < f_2$), the curve presents a negative-slope linear behaviour. Around Λ, both linear branches curve themselves, and intersect at the peak maximum.

In order to quantitatively characterize the peak, Fermat's theorem about local extrema was applied. According to this theorem, the frequency at which $\tau_{\delta}^{S}(\mathrm{f})$ is maximum corresponds to the solutions in f of the following equation:

$$\left.\frac{d\tau_{\delta}^{S}(\mathrm{f})}{df}\right|_{\mathrm{f}=\Lambda} = 0 \qquad (38)$$

Expression (37) was introduced in (38), and the differentiation rules were applied. After solving the obtained equation, and using the fact that $\Lambda \in \mathbb{R}^{+}$ since it is a frequency, the following expression was obtained for Λ, the frequency at which the stabilization time is maximum:

$$\Lambda = \frac{\sqrt{R_0 + R_{ct}}}{2\pi \cdot \tau_{RC} \cdot \sqrt{R_0}} \qquad (39)$$

The right hand side of equation (39) corresponds with the frequency at which the phase angle presents its maximum for a Randles circuit [59]. It can be deduced that for a Randles cell, the stabilization time is maximum at the same frequency at which the phase angle is maximum. The phase angle of the example Randles circuit was

calculated taking the complex argument of expression (32). The obtained phase angle curve was superimposed on figure 4. It can be clearly observed as both, the $\tau_{1\%}^{S}$ curve and the $-\arg(Z)$ curve, reach their maximum at the same frequency, Λ.

In order to obtain the peak height (i.e the maximum stabilization time), the angular frequency, ω, was replaced in equation (35) by $2\pi\Lambda$. After some algebraic manipulations, the following expression was obtained for the maximum stabilization time:

$$\tau_{\delta}^{max} = \tau_{\delta}^{S}(2\pi\Lambda) = -\tau_{RC} \cdot ln\left[\frac{\delta \cdot (2R_0 + R_{ct})}{R_{ct}}\right] \qquad (40)$$

However, for some combinations of R_0 and R_{ct}, even at $f = \Lambda$, the system has already δ-converged to its stationary solution at $t = 0$. For these cases, the above expression returns a negative value. According to the convention selected in the previous section, in these cases, τ_{δ}^{max} will be 0. Therefore, the following modification of equation (40) was considered:

$$\tau_{\delta}^{max} = \begin{cases} -\tau_{RC} \cdot ln\left[\dfrac{\delta \cdot (2R_0 + R_{ct})}{R_{ct}}\right] & if\ R_0 \leq \dfrac{R_{ct}}{2} \cdot \dfrac{\delta + 1}{\delta} \\ 0 & otherwise \end{cases} \qquad (41)$$

It can be observed in expressions (39) and (41), that the value of the peak frequency does not depend on the threshold, δ; whereas the peak height does depend on it. For instance, a $\Delta\delta$ increase in the threshold, causes a $\Delta\tau_{\delta}^{max}$ decrease in the peak height. Therefore, a change in the threshold only causes a vertical translation of the $\tau_{1\%}^{S}$ vs f curve, and does not affect to the peak position. This is consistent with the definition of the threshold concept.

Finally, in order to study the asymptotic behaviour of the curve at low and high frequencies, equation (35) was rewritten in the following way:

$$\tau_{\delta}^{S}(f) = -\tau_{RC} \cdot \left[\ln(\delta) + \frac{1}{2} \cdot ln\left(R_0^2 + \frac{R_{ct} \cdot (2R_0 + R_{ct})}{1 + 4\pi^2 \cdot f^2 \cdot \tau_{RC}^2}\right) + ln(1 + 4\pi^2 \cdot f^2 \cdot \tau_{RC}^2) - ln(2\pi \cdot f \cdot \tau_{RC} \cdot R_{ct})\right] \qquad (42)$$

On the one hand, for high frequencies ($\Lambda \ll f < f_2$), $R_0^2 + \frac{R_{ct} \cdot (2R_0 + R_{ct})}{1 + 4\pi^2 \cdot f^2 \cdot \tau_{RC}^2} \approx R_0^2$ and $1 + 4\pi^2 \cdot f^2 \cdot \tau_{RC}^2 \approx 4\pi^2 \cdot f^2 \cdot \tau_{RC}^2$. Introducing these approximations in expression (42):

$$\tau_\delta^S \cong -\tau_{RC} \cdot ln\left[\frac{2\pi \cdot \delta \cdot R_0 \cdot \tau_{RC}}{R_{ct}}\right] - \tau_{RC} \cdot ln[f] \qquad (43)$$

In a τ_δ^S vs $ln[f]$ semi-log plot, the above expression corresponds to a line equation. Therefore, the high frequency asymptote (HFA) has a slope of $-\tau_{RC}$ (i.e. negative slope) and an y-intercept of $-\tau_{RC} \cdot ln[2\pi \cdot \delta \cdot R_0 \cdot \tau_{RC} \cdot R_{ct}^{-1}]$. The HFA line corresponding to the considered Randles cell example was superimposed on figure 4.

On the other hand, for low frequencies ($f_1 < f \ll \Lambda$), $1 + 4\pi^2 \cdot f^2 \cdot \tau_{RC}^2 \approx 1$. Introducing this approximation in expression (42):

$$\tau_\delta^S \cong -\tau_{RC} \cdot ln\left[\frac{\delta \cdot (R_0 + R_{ct})}{2\pi \cdot \tau_{RC} \cdot R_{ct}}\right] + \tau_{RC} \cdot ln[f] \qquad (44)$$

This expression corresponds to a line equation in the τ_δ^S vs $ln[f]$ semi-log plot. The low frequency asymptote (LFA) has a slope of $+\tau_{RC}$ (i.e. positive slope) and an y-intercept of $-\tau_{RC} \cdot ln[\delta \cdot (R_0 + R_{ct}) \cdot (2\pi \cdot \tau_{RC} \cdot R_{ct})^{-1}]$. The LFA line corresponding to the considered Randles cell example was also superimposed on figure 4.

Equating equation (43) to equation (44), it can be shown that the two asymptotes intersect at $f = \Lambda$. Therefore, the asymptote intersection gives the characteristic frequency of the system, Λ. This fact can be observed in figure 4: HFA and LFA intersect at the same frequency at which the τ_δ^S and $-\arg(Z)$ curves present their maximums.

3.2. Effect of the electrolyte resistance

Figure 5 shows the $\tau_{1\%}^S$ curve for different values of R_0, maintaining constant the other two cell parameters: $R_{ct} = 40\ m\Omega$ and $C_{dl} = 450\ mF$. The dashed line marks the trajectory of the maximum peak. The first observation that can be extracted from it, is that all the HFAs are parallel to each other; and that the LFAs are too. This is consistent with expressions (43) and (44): R_0 has no effect on the slope of the asymptotes. It can also be observed that an increase in R_0 displaces the LFA towards higher frequency values, and the HFA towards lower frequency values. This displacement leads to a higher $\tilde{f}_1$ value, and to a lower $\tilde{f}_2$ value: the $[\tilde{f}_1;\ \tilde{f}_2]$ interval (i.e. where $\tau_{1\%}^S$ is not zero) contracts with a R_0 increase. On the one hand, in the LFA case, when $R_0 \to 0$ the LFA tends to the limit case LFA (i.e. $R_0 = 0$). According to expression (44), the y-intercept of the limit case LFA is $-\tau_{RC} \cdot ln[\delta \cdot R_{ct} \cdot (2\pi \cdot \tau_{RC} \cdot R_{ct})^{-1}]$; and increases in R_0 lead to LFAs with lower y-intercepts. On the other hand, in the HFA case, when $R_0 \to 0$ the HFA diverges (i.e. the HFA is displaced to ∞ frequencies). According to expression (43), the y-intercept of the LFA tends to $+\infty$ when $R_0 \to 0$, and decreases when R_0 increases.

Figure 6 shows the evolution of the peak frequency and height with R_0. It can be observed both, in figure 5 and in figure 6, that an increase in the electrolyte resistance causes a decrease in the characteristic frequency, Λ. For $R_0 \to 0$, the peak frequency tends to $+\infty$: the peak is located at infinite frequencies (i.e. far to the right of the frequency axis). In addition, the characteristic frequency presents an asymptotic behaviour: as it can be seen in expression (39), for large R_0, it tends to $(2\pi \cdot \tau_{RC})^{-1}$. On its side, the peak height also decreases when R_0 increases. According to expression (41), for low values of R_0, the maximum stabilization time tends to $-\tau_{RC} \cdot ln[\delta]$. Increases in R_0, cause the peak height to decrease, until a R_0 value where the peak disappears and the curve is identically equal to 0 at all frequencies. This happens when $R_0 > \frac{R_{ct}}{2} \cdot \frac{\delta+1}{\delta}$.

These results show that the systems with lower electrolyte resistance present higher stabilization times. Therefore, from a stabilization time point of view, special care should be taken when working with systems that exhibit low electrolyte resistances. This is due to the fact that high electrolyte resistances dampen faster the transient response of a Randles system.

3.3. Effect of the charge transfer resistance

Figure 7 shows the $\tau_{1\%}^{S}$ curve for different values of R_{ct}, maintaining constant the other two cell parameters: $R_0 = 10\ m\Omega$ and $C_{dl} = 450\ mF$. As in figure 5, the dashed line marks the trajectory of the maximum peak. It can be observed that the HFAs and LFAs are not parallel to each other, like in the case where R_0 is increased maintaining R_{ct} and C_{dl} constant. Instead, the absolute value of their slope rises when R_{ct} is increased. This is consistent with expressions (43) and (44), according to which the absolute value of the asymptotes' slope is $\tau_{RC} = R_{ct} \cdot C_{dl}$. It can also be observed that an increase in R_{ct} displaces the $\tilde{f}_1$ value towards lower frequencies, while it does not affect to the $\tilde{f}_2$ value: the $[\tilde{f}_1;\ \tilde{f}_2]$ interval (i.e. where $\tau_{1\%}^{S}$ is not zero) expands when R_{ct} increases.

Figure 8 gives the evolution of the peak frequency and height with R_{ct}. On the one hand, as it can be seen in figures 7 and 8, an increase in the charge transfer resistance leads to a drop of the characteristic frequency, Λ. As in the R_0 case, when $R_{ct} \to 0$, the peak frequency tends to $+\infty$: the peak is located at infinite frequencies (i.e. far to the right of the frequency axis). Unlike the R_0 case, Λ does not present any asymptotic behaviour for $R_{ct} \to +\infty$: for large charge transfer resistances, Λ dercreases as $R_{ct}^{-1/2}$. On the other hand, the peak height increases with R_{ct}. According to expression (41), τ_{δ}^{max} increases unboundly with R_{ct}. For very low values of the charge transfer

resistance ($R_{ct} < \frac{2\delta}{\delta+1} \cdot R_0$), the peak disappears and the curve is identically equal to 0 at all frequencies.

These results show that the systems with higher charge transfer resistance present higher stabilization times. Consequently, from a stabilization time point of view, special care should be taken when working with systems that exhibit high charge transfer resistances. This is due to the fact that high charge transfer resistances result in Randles systems with high time constants. And a higher time constant causes the transient response to dampen slower (i.e. higher stabilization time).

3.4. Effect of the double layer capacitance

Finally, the $\tau_{1\%}^{S}$ curves for different values of C_{dl}, maintaining constant the other two cell parameters ($R_0 = 10\ m\Omega$ and $R_{ct} = 40\ m\Omega$) are represented in figure 9. As in figures 5 and 7, the dashed line locates the trajectory of the maximum peak. As in the R_{ct} case, the HFAs and LFAs are not parallel to each other: the absolute value of their slope rises with C_{dl}. This is consistent with expressions (43) and (44), according to which the absolute value of the asymptotes' slope is $\tau_{RC} = R_{ct} \cdot C_{dl}$. Furthermore, an increase in C_{dl} displaces both, the $\tilde{f}_1$ value and the $\tilde{f}_2$ value, towards lower frequencies, maintaining constant the $\tilde{f}_2 - \tilde{f}_1$ distance.

Figure 10 shows the evolution of the peak frequency and height with C_{dl}. As it can be observed in figures 9 and 10, an increase in the double layer capacitance causes the characteristic frequency, Λ, to drop. As in the R_0 and R_{ct} cases, when $C_{dl} \to 0$, the peak frequency tends to $+\infty$: the peak is located at infinite frequencies (i.e. far to the right of the frequency axis). In the C_{dl} case, like in the R_{ct} case, Λ does not present any asymptotic behaviour for $C_{dl} \to +\infty$: for large double layer capacitance, Λ dercreases as C_{dl}^{-1}. On its side, the peak height increases with C_{dl}. According to expression (41), τ_{δ}^{max} increases unboundly with C_{dl}. Unlike the cases of the electrolyte and the charge transfer resistances, in the double layer capacitance case, the peak only disappears completely for $C_{dl} = 0$.
These results show that the systems with higher double layer capacitances present higher stabilization times. Consequently, from a stabilization time point of view, special care should be taken when working with systems that exhibit high double layer capacitances. As in the charge transfer resistance case, this is due to the fact that high double layer capacitances result in Randles systems with high time constants. And a higher time constant causes the transient response to dampen slower (i.e. higher stabilization time).

4. Application to examples of real systems

In this section, the results derived in this work are going to be applied to different examples of real systems available in literature. When working with real systems, it is a common practice to replace the capacitance of the Randles equivalent circuit by a constant phase element [34]. For this reason many works characterize the studied system by giving R_0, R_{ct}, Q and α. Where Q denotes the pseudo-capacitance, and α is the exponent of the constant phase element. In order to apply this work's results, the equivalent double layer capacitance of such systems was obtained using Brug's formula [60].

Table 1 sums up the parameter values of different real system examples available in literature. Expression (41) was applied in each case in order to obtain the theoretical maximum stabilization time, associated to a 1% threshold. The obtained results are given in the last column of the table. As it can be observed, the maximum stabilization time ranges from a few milliseconds to more than an hour. This shows the importance of estimating the required stabilization time for each system individually.

5. Conclusions

In conclusion, a theoretical dynamic model of a Randles cell under galvanostatic sinusoidal perturbation has been successfully developed in this work. This model can be used to estimate, from a theoretical point of view, the required stabilization time for performing EIS measurements in a Randles-like system. It should be noted that the system's parameters are needed in order to estimate the required stabilization time. Therefore, in practice, the order of magnitude of the system's parameters has to be known in order to be able to use this method. So, for a completely new system, a preliminary study has to be done: A preliminary EIS measurement should be done with the default measurement parameters. From this preliminary EIS spectrum, the order of magnitude of the system's parameters can be estimated, and then, the required stabilization time can be deduced. This stabilization time can then be used for the subsequent EIS measurements of the system. The preliminary EIS measurement can be avoided if the system's parameters are estimated using chronoamperometric measurements. Another potential application of this method is to check a posteriori if the selected stabilization time is long enough: once the EIS measurement has already been performed, the required stabilization time is estimated using the system's parameters. If the required stabilization time is shorter than the stabilization time selected for performing the measurement, then the results can be accepted; on the contrary, if the required stabilization time is longer than the stabilization time selected for performing the measurement, then the results cannot be accepted and the measurement has to be repeated using the estimated required stabilization time.

This work focuses on the simplest case: the simplified Randles cell. Nevertheless, the theoretical framework (Characteristic ODE, Sinusoidal forcing, Transient component, Stabilization time) presented here can be applied to any system, however complex it may be. The only difference is that while analytical solutions can be deduced for simple systems, as the simplified Randles cell; more complex systems may require the use of numerical methods.

6. Nomenclature

Latin symbols

$\arg(Z)$	Impedance argument (rad)
C	Capacitance (F)
C_{dl}	Double layer capacitance (F)
f	Frequency (Hz)
I	Current (A)
I_{DC}	DC current (A)
j	Imaginary unit
R	Resistance (Ω)
R_0	Electrolyte resistance (Ω)
R_{ct}	Charge transfer resistance (Ω)
t	Time (s)
U	Voltage (V)
U_{DC}	DC voltage (V)
Z	Complex impedance (Ω)
$\lvert Z \rvert$	Impedance modulus (Ω)
Z'	Real part of the complex impedance (Ω)
Z''	Imaginary part of the complex impedance (Ω)

Greek symbols

ΔI	Galvanostatic perturbation amplitude (A)
ΔU_{SS}	Amplitude of the stationary AC component of the voltage signal (V)
δ	Convergence threshold $(\%)$
Λ	Frequency at which the stabilization time is maximum (Hz)
τ_{RC}	RC time constant (s)
τ_δ^{max}	Maximum stabilization time associated to a δ threshold (s)
τ_δ^S	Stabilization time associated to a δ threshold (s)
ω	Angular frequency $(rad \cdot s^{-1})$

Subscripts

ct	Related to charge transfer
DC	DC component
dl	Related to the double layer
SS	Related to the stationary state
tot	Related to the whole cell
$trans$	Related to the transient

7. Acknowledgments

The authors are very grateful to the Generalitat Valenciana (Vali+d postdoctoral grant APOSTD/2018/001), to the Ministerio de Economia y Competitividad (Project CTQ2015-65202-C2-1-R), to the European Regional Development Fund (FEDER) and to the European Social Fund, for their economic support.

8. Bibliography

[1] Y. Li, L. Xu, M. Jia, L. Cui, J. Gao and X.J. Jin, J. Electrochem. Soc., **165**, E303 (2018).

[2] Q. Liu, L. Zang, C. Yang, C. Wei, J. Qiu, C. Liu and X. Xu, J. Electrochem. Soc., **165**, A1515 (2018).

[3] A. Di Blasi, C. Busacca, O. Di Blasi, N. Briguglio and V. Antonucci, J. Electrochem. Soc., **165**, A1478 (2018).

[4] M. Wetjen, S. Solchenbach, D. Pritzl, J. Hou, V. Tileli and H.A. Gasteiger, J. Electrochem. Soc., **165**, A1503 (2018).

[5] L.D. Ellis, J.P. Allen, I.G. Hill and J.R. Dahn, J. Electrochem. Soc., **165**, A1529 (2018).

[6] B.S. Jayathilake, E.J. Plichta, M.A. Hendrickson and S.R. Narayanan, J. Electrochem. Soc., **165**, A1630 (2018).

[7] A. Sahoo, B. Deka and Y. Sharma, J. Electrochem. Soc., **165**, A1610 (2018).

[8] W. Tao, H. Zhang, T. Jia, S. Luo, Q. Hou, Y. Wang, G. Shi and B. Xu, J. Electrochem. Soc., **165**, A1574 (2018).

[9] S.C. Barman, M.F. Hossain, H. Yoon and J.Y. Park, J. Electrochem. Soc., **165**, B296 (2018).

[10] A. Thomas and K.G. Kumar, J. Electrochem. Soc., **165**, B351 (2018).

[11] S.M. Ali and H.A. Al-lehaibi, J. Electrochem. Soc., **165**, B345 (2018).

[12] C. Villena, D. Punjabi, C.M. Casado, B. Alonso, J. Losada and M.P. García-Armada, J. Electrochem. Soc., **165**, B310 (2018).

[13] E.A. Astafev, A.E. Ukshe and Y.A. Dobrovolsky, J. Electrochem. Soc., **165**, F604 (2018).

[14] R. Pavlicek, S.C. Barton, N. Leonard, H. Romero, S. McKinney, G. McCool, A. Serov, D. Abbott, P. Atanassov and S. Mukerjee, J. Electrochem. Soc., **165**, F589 (2018).

[15] J.J. Giner-Sanz, E.M. Ortega and V. Pérez-Herranz, J. Power Sources, **379**, 328 (2018).

[16] J.J. Giner-Sanz, E.M. Ortega and V. Pérez-Herranz, J. Power Sources, **381**, 84 (2018).

[17] H. Wang and S.A. Barnett, J. Electrochem. Soc., **165**, F564 (2018).

[18] K. Neuhaus, R. Dolle and H.D. Wiemhöfer, J. Electrochem. Soc., **165**, F533 (2018).

[19] M. Mandal, A. Valls, N. Gangnus and M. Secanell, J. Electrochem. Soc., **165**, F543 (2018).

[20] J.J. Giner-Sanz, E.M. Ortega and V. Pérez-Herranz, Fuel Cells, **17**, 391 (2017).

[21] J.J. Giner-Sanz, E.M. Ortega and V. Pérez-Herranz, J. Electrochem. Soc., **165**, E488 (2018).

[22] L. Zhu, W. Zhang, T. Zhang, J. Qiu, J. Cao and F. Wang, J. Electrochem. Soc., **165**, C469 (2018).

[23] K. Hoshino, S. Furuya and R.G. Buchheit, J. Electrochem. Soc., **165**, C461 (2018).

[24] E. Huttunen-Saarivirta, E. Ghanbari, F. Mao, P. Rajala, L. Carpén and D.D. Macdonald, J. Electrochem. Soc., **165**, C450 (2018).

[25] D. Liu, Y. Song, D. Shan and E. Han, J. Electrochem. Soc., **165**, C412 (2018).

[26] C.D. Lee, E.M. Hudak, J.J. Whalen III, A. Petrossians and J.D. Weiland, J. Electrochem. Soc., **165**, G3015 (2018).

[27] Y. Jian, C. Lee, F. Jan and G. Wang, J. Electrochem. Soc., **165**, H449 (2018).

[28] J.J. Giner-Sanz, E.M. Ortega and V. Pérez-Herranz, Fuel Cells, **16**, 469 (2016).

[29] J.J. Giner-Sanz, E.M. Ortega and V. Pérez-Herranz, J. Electrochem. Soc., **164**, H918 (2017).

[30] J.J. Giner-Sanz, E.M. Ortega and V. Pérez-Herranz, Electrochim. Acta, **209**, 254 (2016).

[31] J.J. Giner-Sanz, E.M. Ortega and V. Pérez-Herranz, Int. J. Hydrogen Energ., **40**, 11279 (2015).

[32] J.J. Giner-Sanz, E.M. Ortega and V. Pérez-Herranz, Electrochim. Acta, **186**, 598 (2015).

[33] J.J. Giner-Sanz, E.M. Ortega and V. Pérez-Herranz, Electrochim. Acta, **211**, 1076 (2016).

[34] M.E. Orazem and B. Tribollet, *Electrochemical Impedance Spectroscopy*, John Wiley & Sons, Hoboken (2008).

[35] E. Barsoukov and J.R. Macdonald, *Impedance spectroscopy. Theory, experiment and applications*, 2nd ed., John Wiley & Sons, New York (2005).

[36] J.J. Giner-Sanz, E.M. Ortega and V. Pérez-Herranz, Electrochim. Acta, **174** 1290 (2015).

[37] Y.F Pulido, C. Blanco, D. Anseán, V.M. García, F. Ferrero and M. Valledor, Measurement, **106**, 1 (2017).

[38] J.E.B. Randles, Discuss. Faraday Soc., **1**, 11 (1947).

[39] D.A. Harrington and P.V.D. Driessche, Electrochim. Acta, **56**, 8005 (2011).

[40] D.V. Ribeiro and J.C.C. Abrantes, Constr. Build. Mater., **111**, 98 (2016).

[41] G. Liu, Y. Zhang, M. Wu and R. Huang, Constr. Build. Mater., **157**, 357 (2017).

[42] J. Li, N. Birbilis and R.G. Buchhleit, Corros. Sci., **101**, 155 (2015).

[43] R.H. Tammam and M.M. Saleh, J. Electroanal. Chem., **794**, 189 (2017).

[44] R. Garcia-Garcia, J.G. Rivera, R. Antaño-Lopez, F. Castañeda-Olivares and G. Orozco, Int. J. Hydrogen Energ., **41**, 4660 (2016).

[45] M. Qu, S. Wang, L. Li and X. Liu, Mater. Lett., **207**, 187 (2017).

[46] M. Pérez-Page and V. Pérez-Herranz, Int. J. Hydrogen Energ., **39**, 4009 (2014).

[47] M. Sindhuja, N.S. Kumar, V. Sudha and S. Harinipriya, J. Energy Storage, **7**, 136 (2016).

[48] S. Cruz-Manzo and R. Chen, J. Electroanal. Chem., **694**, 45 (2013).

[49] S.V.D. Lima and H.P.D. Oliveira, Colloid. Surface. A, **364**, 132 (2010).

[50] N.E.A. Cousens and A.R. Kucernak, Electrochem. Comm., **31**, 63 (2013).

[51] E. García-Macías, A. Downey, A. D'Alessandro, R. Castro-Triguero, S. Laflamme and F. Ubertini, Sensor. Actuat. A-Phys., **260**, 45 (2017).

[52] R. Vergaz, D. Barrios, J.M. Sánchez-Pena, C. Pozo-Gonzalo, M. Salsamendi and J.A. Pomposo, Displays, **29**, 401 (2008).

[53] J.G. Lee, J.Y. Lee, J. Yun, Y. Lee, S. Lee, S.J. Shin and T.D. Chung, Electrochem. Comm., **76**, 75 (2017).

[54] C. Roldan-Cruz, J. Carmona-Ascencio, E.J. Vernon-Carter and J. Alvarez-Ramirez, Colloid. Surface. A, **495**, 125 (2016).

[55] Gamry Instruments, *Basics of Electrochemical Impedance Spectroscopy*, Application note, Warminster (2016).

[56] P.A. Foerster, Properties of Combined Sinusoids, *Precalculus with Trigonometry: Concepts and Applications*, 3rd edition, Springer Science & Business Media, New York (2003).

[57] E. Lindelöf, Comptes rendus hebdomadaires des séances de l'Académie des sciences, **116**, 454 (1894).

[58] A.L. Rabenstein, *Introduction to Ordinary Differential Equations: With Applications*, Academic Press, New York (2014).

[59] J.P. Diard, B. Le Gorrec and C. Montella, Circuits made of Resistors and Capacitors, *Handbook of Electrochemical Impedance Spectroscopy*, Bio-Logic, Paris (2011).

[60] G.J. Brug, A.L.G. Van Den Eeden, M. Sluyters-Rehbach and J.H. Sluyters, J. Electroanal. Chem., **176**, 275 (1984).

Table 1. Theoretical maximum stabilization time, associated to a $\mathbf{1}\%$ threshold, for different real systems extracted from literature

System	R_0	R_{ct}	C_{dl}	$\tau_{1\%}^{max}$
Cathodic hydrogen evolution reaction on polycrystalline rhenium [43]	$1.8\ \Omega$	$155\ \Omega$	$2.9\ \mu\mathrm{F}$	$2.1\ \mathrm{ms}$
W electrodes [44]	$2.0\ \Omega$	$4.6\ k\Omega$	$0.19\ \mathrm{F}$	$1.1\ \mathrm{hr}$
Depassivation of carbon steel [40]	$212\ \Omega$	$72\ k\Omega$	$25\ \mu\mathrm{F}$	$1.4\ \mathrm{min}$
Individual cell of a PEM fuel cell stack [35]	$6.0\ m\Omega$	$38\ m\Omega$	$0.21\ \mathrm{F}$	$34\ \mathrm{ms}$
Urea oxidation on Ni oxide nanoparticles modified glassy carbon electrode [42]	$32\ \Omega$	$2.3\ k\Omega$	$7.4\ \mu\mathrm{F}$	$78\ \mathrm{ms}$
Viologen-based electrochromic display [51]	$116\ \Omega$	$32\ k\Omega$	$9.4\ \mu\mathrm{F}$	$14\ \mathrm{s}$
Gum complexation process [53]	$48\ \Omega$	$44\ k\Omega$	$3.1\ m\mathrm{F}$	$10\ min$

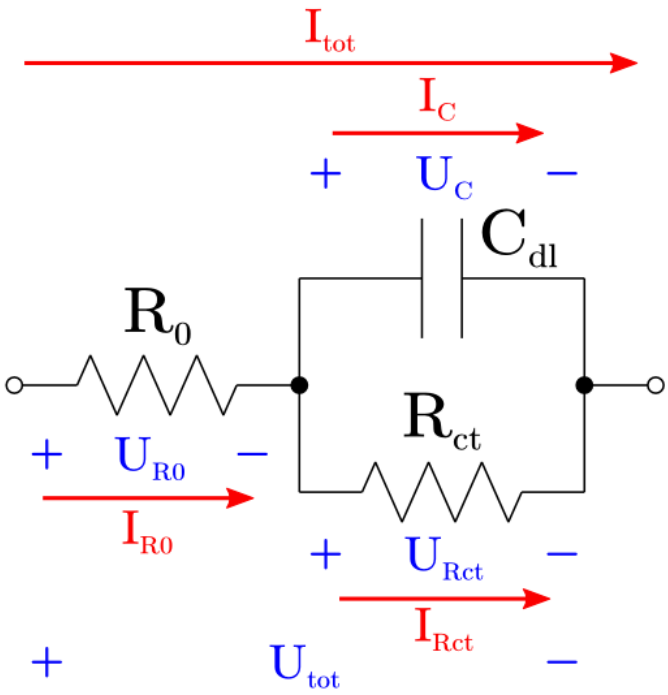

Figure 1. Variables and parameters of the simplified Randles cell

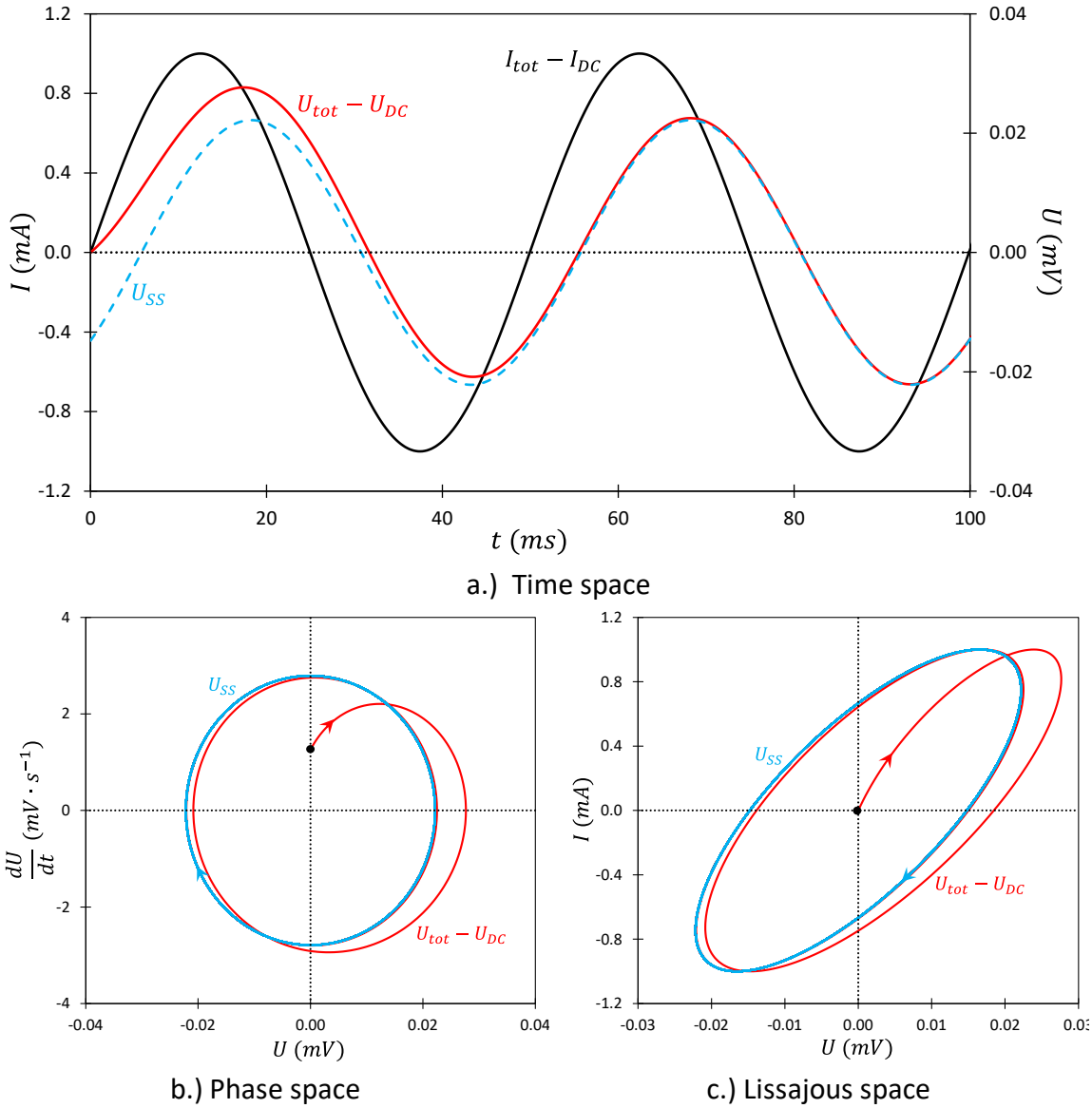

Figure 2. Simulated transient for a particular Randles cell ($\boldsymbol{R_0 = 10\ m\Omega}$, $\boldsymbol{R_{ct} = 40\ m\Omega}$ and $\boldsymbol{C_{dl} = 450\ m\mathrm{F}}$) and a particular perturbation ($\boldsymbol{\Delta \mathrm{I} = 1\ \mathrm{mA}}$ and $\boldsymbol{\mathrm{f} = 20\ \mathrm{Hz}}$), in different spaces

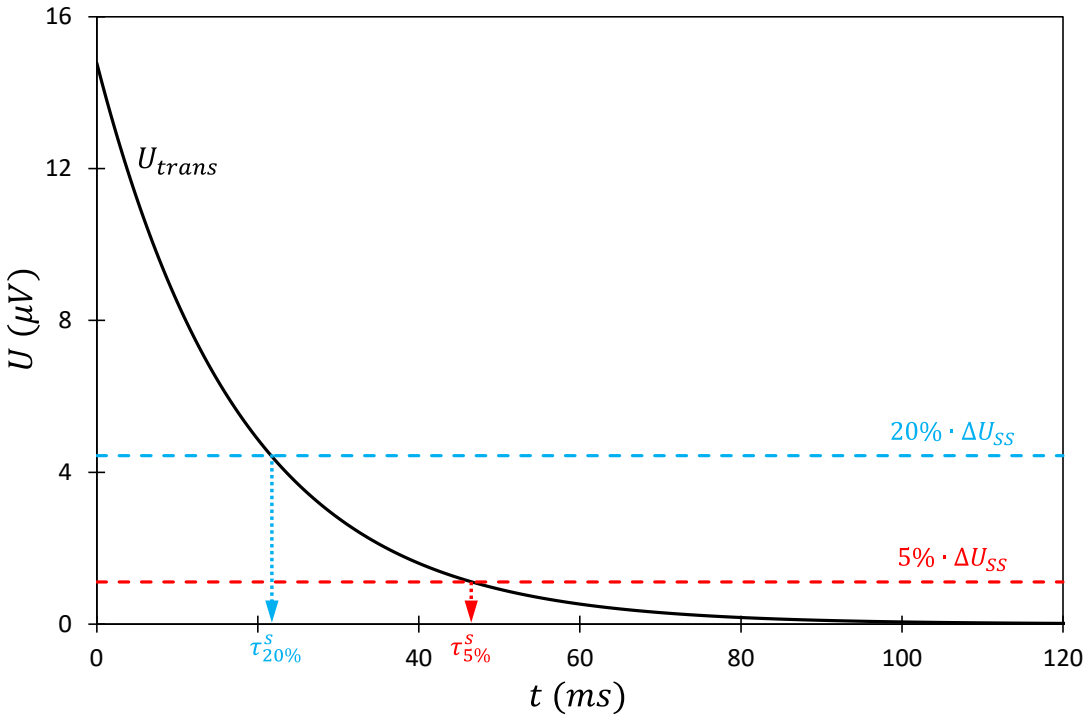

Figure 3. Simulated transient component for a particular Randles cell ($\boldsymbol{R_0 = 10\ m\Omega}$, $\boldsymbol{R_{ct} = 40\ m\Omega}$ and $\boldsymbol{C_{dl} = 450\ m}$**F**) and a particular perturbation ($\boldsymbol{\Delta I = 1\ mA}$ and $\boldsymbol{f = 20\ Hz}$)

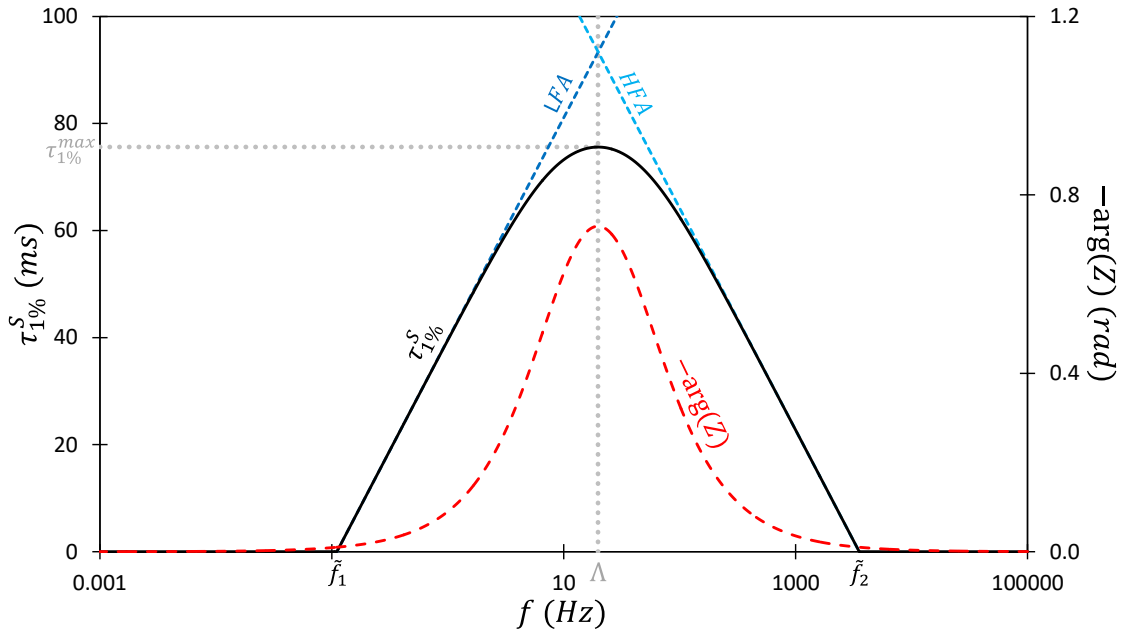

Figure 4. Effect of the perturbation frequency on the stabilization time associated to a $\mathbf{1}\%$ threshold, for an example Randles cell ($\boldsymbol{R_0 = 10\ m\Omega}$, $\boldsymbol{R_{ct} = 40\ m\Omega}$ and $\boldsymbol{C_{dl} = 450\ m\mathrm{F}}$)

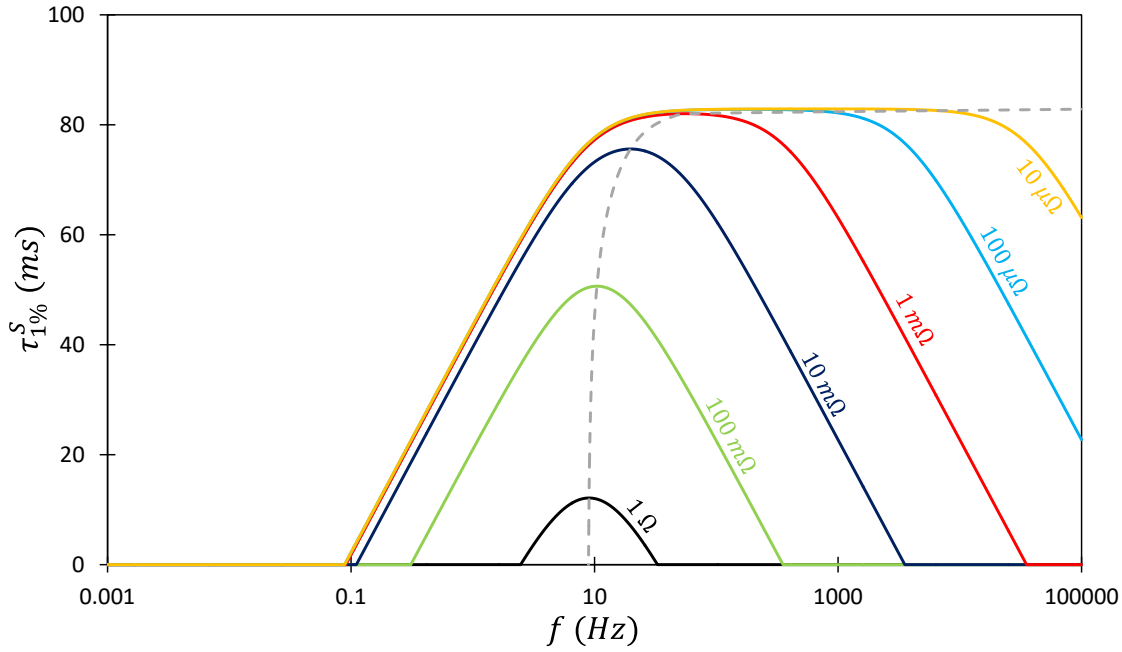

Figure 5. Effect of the electrolyte resistance on the stabilization time associated to a $\mathbf{1}\%$ threshold, maintaining the other two parameters constant ($\mathbf{R_{ct} = 40\ m\Omega}$ and $\mathbf{C_{dl} = 450\ mF}$)

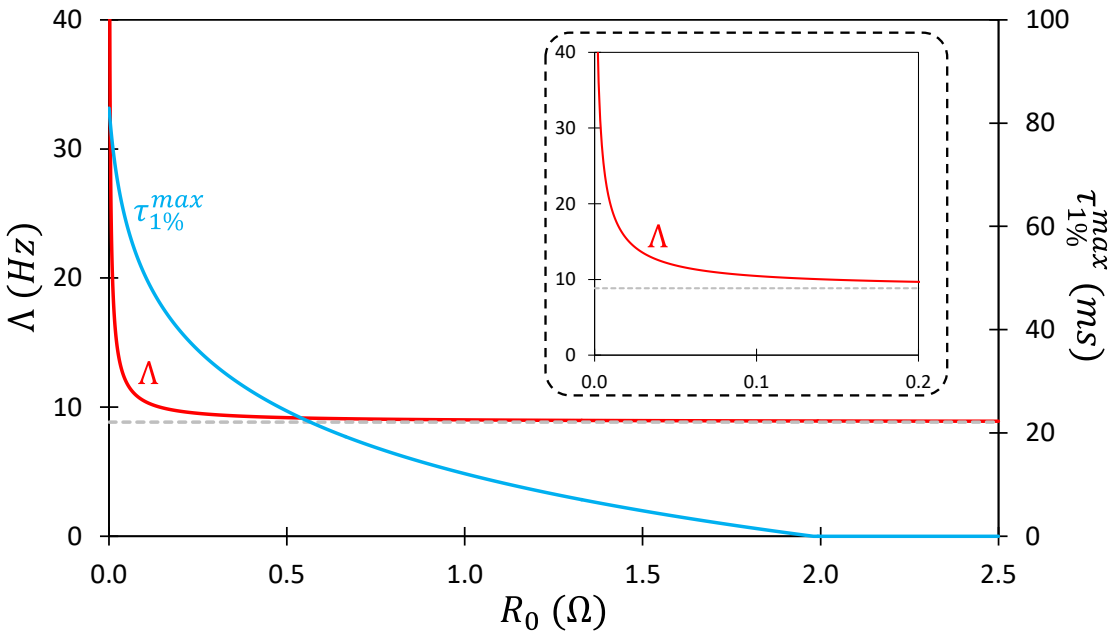

Figure 6. Effect of the electrolyte resistance on the maximum stabilization time associated to a $\mathbf{1\%}$ threshold, and on the corresponding peak frequency, maintaining the other two parameters constant ($\mathbf{R_{ct} = 40\ m\Omega}$ and $\mathbf{C_{dl} = 450\ mF}$)

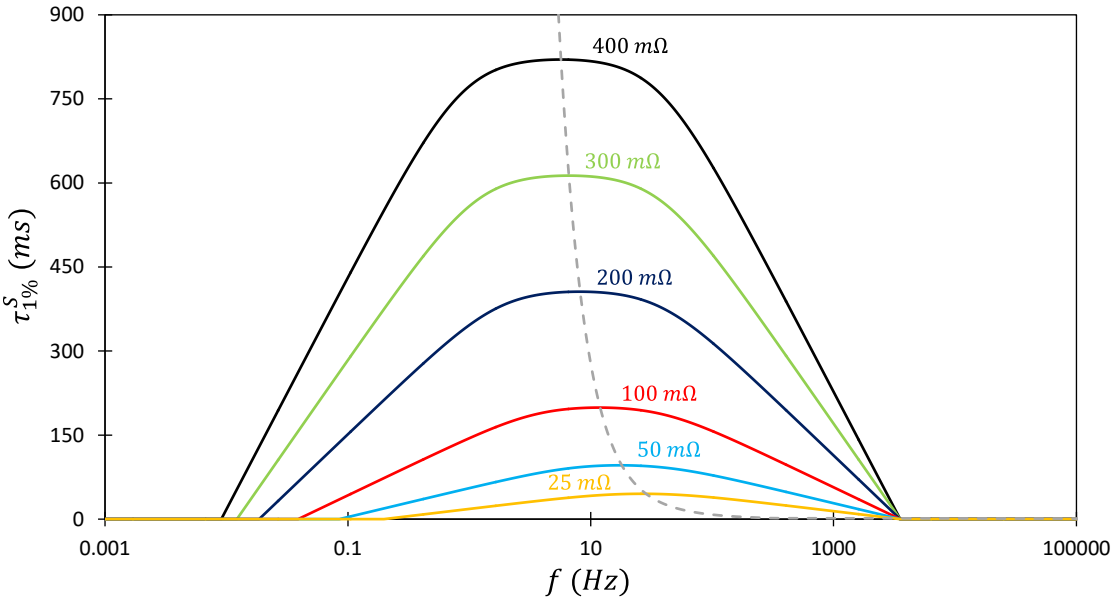

Figure 7. Effect of the charge transfer resistance on the stabilization time associated to a $\mathbf{1}\%$ threshold, maintaining the other two parameters constant ($\boldsymbol{R_0 = 10\ m\Omega}$ and $\mathbf{C_{dl} = 450\ mF}$)

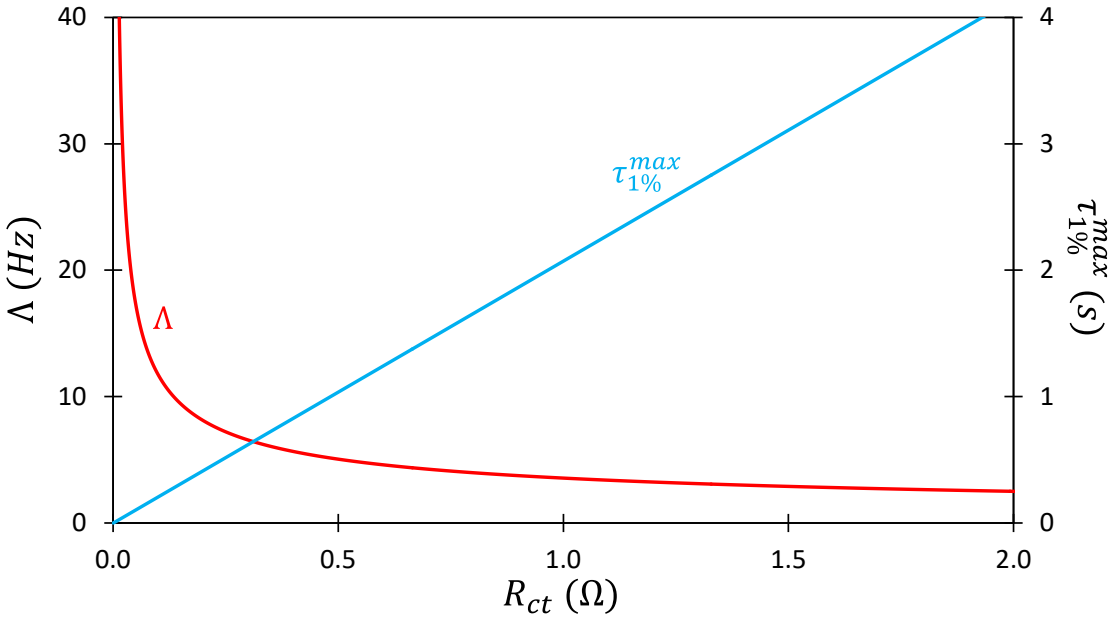

Figure 8. Effect of the charge transfer resistance on the maximum stabilization time associated to a $\mathbf{1\%}$ threshold, and on the corresponding peak frequency, maintaining the other two parameters constant ($\boldsymbol{R_0 = 10\ m\Omega}$ and $\mathbf{C_{dl} = 450\ mF}$)

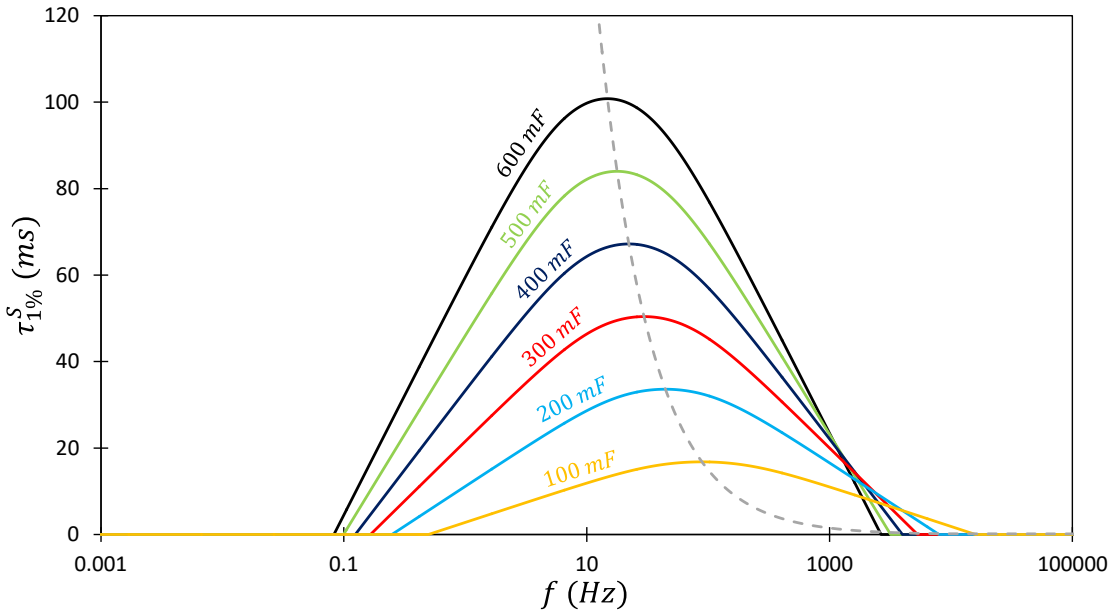

Figure 9. Effect of the double layer capacitance on the stabilization time associated to a $\mathbf{1}\%$ threshold, maintaining the other two parameters constant ($\boldsymbol{R_0 = 10\ m\Omega}$ and $\boldsymbol{R_{ct} = 40\ m\Omega}$)

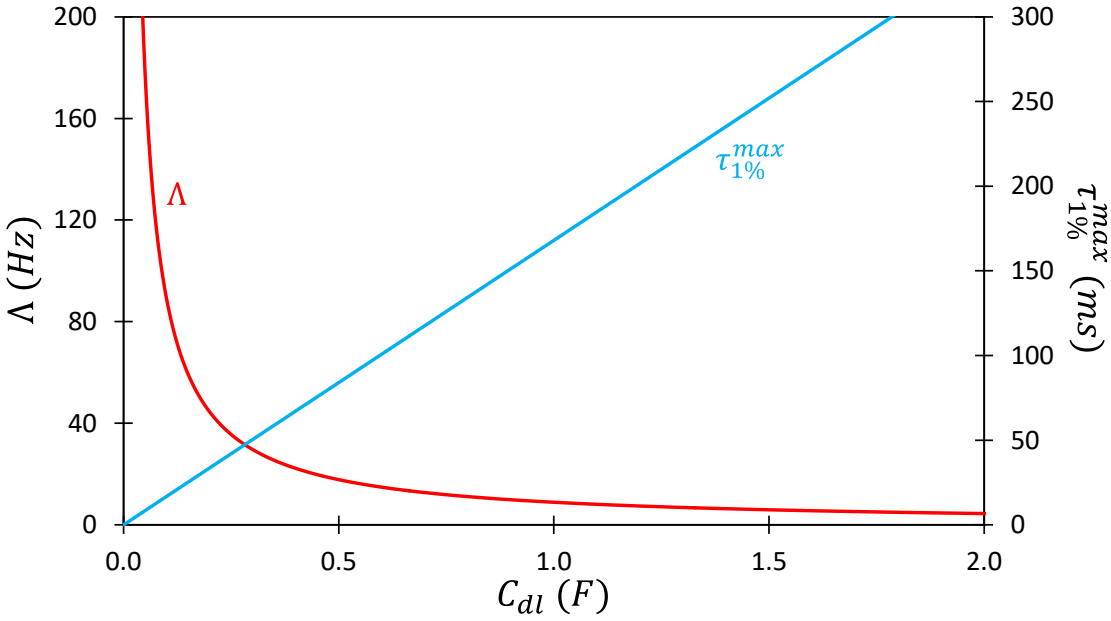

Figure 10. Effect of the double layer capacitance on the maximum stabilization time associated to a $\mathbf{1}\%$ threshold, and on the corresponding peak frequency, maintaining the other two parameters constant ($\boldsymbol{R_0 = 10\ m\Omega}$ and $\boldsymbol{R_{ct} = 40\ m\Omega}$)